On the statistical stability of the M2 barotropic and baroclinic tidal characteristics from along-track TOPEX/Poseidon satellite altimetry analysis

Loren Carrère, Christian Leprovost, Florent Lyard

▶ **To cite this version:**

Loren Carrère, Christian Leprovost, Florent Lyard. On the statistical stability of the M2 barotropic and baroclinic tidal characteristics from along-track TOPEX/Poseidon satellite altimetry analysis. Journal of Geophysical Research, 2004, 109 (C03033), pp.13. 10.1029/2003JC001873 . hal-00765720

HAL Id: hal-00765720
https://hal.science/hal-00765720

Submitted on 10 Jun 2014

HAL is a multi-disciplinary open access archive for the deposit and dissemination of scientific research documents, whether they are published or not. The documents may come from teaching and research institutions in France or abroad, or from public or private research centers.

L'archive ouverte pluridisciplinaire **HAL**, est destinée au dépôt et à la diffusion de documents scientifiques de niveau recherche, publiés ou non, émanant des établissements d'enseignement et de recherche français ou étrangers, des laboratoires publics ou privés.

On the statistical stability of the M_2 barotropic and baroclinic tidal characteristics from along-track TOPEX/Poseidon satellite altimetry analysis

Loren Carrère, Christian Le Provost, and Florent Lyard

Laboratoire d'Etude en Géophysique et Océanographie Spatiales, Unite Mixte CNRS-CNES-IRD-UPS, Toulouse, France

Received 27 March 2003; revised 10 July 2003; accepted 11 November 2003; published 20 March 2004.

[1] An along-track analysis of 7 years of TOPEX/Poseidon (T/P) data has been performed on the global ocean over the period 1993–1999. Such long time series allow us to determine the semidiurnal tidal component very accurately, while resolving the aliasing problems, at least for the main tidal wave M_2. As already inferred by other authors, this along-track analysis detects the surface signatures of the internal tides signal that maintains coherence with the M_2 astronomical forcing. By analyzing the T/P data in different periods of 3 years or more, the stability of the M_2 tidal characteristics is demonstrated for the barotropic component as well as for the baroclinic signal observed in the altimetric data. This stability varies with location. For the barotropic component the dispersion of the results as a function of the length and period of analysis is only significant over the areas of ocean mesoscale activity (noise impact) and of large barotropic tidal signal (separating the different components of the tidal signal proves difficult). The baroclinic tidal signal appears to be surprisingly stable over many areas located around strong topographic gradients like submarine ridges. A methodology has been developed to draw a map of these areas. This can be of help for ocean modelers to specify areas of higher vertical mixing associated with internal tidal wave activity and for those who assimilate altimetric data in their models by giving guidance on where to increase the uncertainty of the altimeter data over these areas. *INDEX TERMS:* 4544 Oceanography: Physical: Internal and inertial waves; 4560 Oceanography: Physical: Surface waves and tides (1255); 4556 Oceanography: Physical: Sea level variations; *KEYWORDS:* barotropic-baroclinic tides, statistical stability, altimetry

Citation: Carrère, L., C. Le Provost, and F. Lyard (2004), On the statistical stability of the M_2 barotropic and baroclinic tidal characteristics from along-track TOPEX/Poseidon satellite altimetry analysis, *J. Geophys. Res.*, *109*, C03033, doi:10.1029/2003JC001873.

1. Introduction

[2] High-precision satellite altimetry has allowed getting very accurate solutions for ocean tides at the global scale [*Le Provost et al.*, 1995; *Le Provost*, 2001]. The main difficulty encountered in extracting the tidal characteristics from the altimetric signal is related to the repeat cycle period of the altimeter satellites. Their low-frequency sampling of the ocean topography results in aliasing of the high-frequency signals into much longer periods. The TOPEX/Poseidon (T/P) repeat cycle period of 9.9156 days results in an aliasing of the semidiurnal M_2 lunar and S_2 solar tide at 62.10 days and 58.74 days, respectively, and the diurnal K_1 component at 173.19 days. Strict application of Rayleigh's criterion for separating the characteristics of these waves in the T/P spectrum requires 3 years to separate M_2 from S_2 and 9 years to isolate K_1 from the semiannual oceanic signal. This difficulty was overcome at the very beginning of the T/P data analysis by estimating tides in bins with a typical size of 3°, which is a little larger than the T/P longitudinal sampling at low latitude. This allows one to combine information from neighboring tracks and thus increase the number of observations per T/P repeat cycle [*Schrama and Ray*, 1994]. Note that this procedure corresponds to differential improvements to a reference tidal model, allowing one to preserve the scales smaller than 3° bins included in the reference.

[3] After a few years of the T/P mission, it became possible to analyze the altimetric data along track (one point every 7 km). These analyses revealed that altimetry detects surface wave features in M_2 that are too high frequency in space to be barotropic tide features. Except for areas subject to ocean mesoscale activity linked to strong ocean currents and over strong topographic features (continental shelves and ridges), it is likely that we are detecting the part of the internal tides that maintains coherence with the astronomical forcing [*Ray and Mitchum*, 1997].

[4] Now, with more than 10 years of T/P data, determination of the tidal contribution to sea level variability through direct along-track analysis is even more accurate,

Copyright 2004 by the American Geophysical Union.
0148-0227/04/2003JC001873

because of the increase of the signal-to-noise ratio, and more effective separation of the different tidal components.

[5] The aim of this paper is to investigate the convergence and stability of the tidal characteristics directly deduced from along-track analysis of the T/P data and to locate the areas where these characteristics are the most stable. These investigations will consider the barotropic and baroclinic tides. The focus will be on the major M_2 tidal component.

2. Data and Method

2.1. Data Set

[6] The basic data set used in this study is the sea surface topography measured by the T/P satellite sampled along track every 7 km with a repeat period of 9.9156 days. A reference set of geographical locations has been chosen, based on the 7-km samples of the tracks of cycle 11. Time series have been built by interpolating the original T/P data along track and cross track in order to fit exactly to these locations. The T/P data were previously corrected for instrumental noise, orbit determination error and geophysical errors, including the loading tide (CSR3.0) and the inverse barometer effect. Cycles 11 to 255 have been used, so that the time series thus constructed correspond to approximately 7 years of data, from 1993 to 1999.

2.2. Harmonic Analysis Method

[7] To extract tides from this data set, the following decomposition of the sea surface height has been considered:

$$h(\bar{x},t) = h_0(\bar{x}) + h_1(\bar{x},t) + h_2(\bar{x},t) + \varepsilon(\bar{x},t)$$

where

- $\bar{x}$ geographic location of the measurement on the sphere;
- h sea surface height already cleared from the inverse barometer effect and loading tides (CSR3.0 correction), but not ocean tides, of course;
- h_0 mean height;
- h_1 barotropic tidal height;
- h_2 coherent baroclinic tide, which represents the baroclinic signal phase-locked (i.e., coherent) with the tide generating forcing;
- ε "residual (for us)" signal, i.e., the remaining ocean signal, including the noncoherent part of the baroclinic tide.

[8] The tidal contribution h_T, which is the sum of the barotropic h_1 and the baroclinic h_2 contributions, is taken as

$$h_T(x,y,t) = \sum_{i=1}^{N} f_i(t) A_i(x,y) \cos\left(\omega_i t - g_i(x,y) + (V_0+u)_i(t)\right)$$

where

- A_i amplitude of the ith wave;
- ω_i angular velocity of the ith wave;
- g_i phase lag of the ith wave compared to the crossing of the Greenwich meridian by the disrupting star;
- V_0 phase of the tide generating body at the time origin;
- $u_i(t)$ phase nodal correction coefficient for the ith wave;
- $f_i(t)$ amplitude nodal correction coefficient for the ith wave.

[9] The aim of this paper is to investigate the statistical stability of the A_i and g_i characteristics of the barotropic and phase-locked baroclinic tides over the 7-year span of T/P considered.

[10] Two methods are generally used to process such satellite data sets in terms of tidal analysis: the harmonic method and the response method. We have used the first of these, because it preserves the local characteristics of the information; although limited by the aliasing problem, this method has the advantage of delivering independent values for the tidal components without assuming smooth admittance on the wave species. It must also be noted that the orthotides analysis generally gives very similar results to the harmonic method, at least for waves that do not pose an aliasing problem: M_2, N_2, S_2 [see *Kantha and Tierney*, 1997].

[11] We thus analyze the T/P signal generated at each nominal point chosen along the different tracks. The analysis code used here [*Ponchaut et al.*, 2001] allows us to isolate as many waves as we wish. The standard is 77 waves. However, analyzing 77 waves with a time series of only at most 244 points (7 years of T/P data) is quite tight from the mathematical point of view to solve the least squares problem of the harmonic analysis method. We thus have considered only 20 constituents: the six main tidal waves (M_2, S_2, N_2, K_1, O_1, Q_1), some nonlinear ones, introduced for further coastal studies (M_4, MS_4, N_4, M_6), and some small astronomical waves ($2N_2$, μ_2, ν_2, L_2, T_2, K_2, S_1, OO_1, J_1, P_1).

2.3. Separation of the Barotropic and Baroclinic Signals

[12] As mentioned in section 2.2, the baroclinic signal is composed of two parts: a part phase-locked with the barotropic tide and a part which is not coherent with the barotropic signal, although it also owes its existence to it. This incoherent signal is due to the temporal and spatial variability of the oceanic environment, which results in stratification and large-scale oceanic current modifications and thus in internal wave variability. It also includes the solitons generated and the instable internal modes.

[13] To isolate the barotropic part of the signal, several methods can be applied, ranging from the use of solutions derived from mathematical models of the barotropic tides to a filtering of the long wavelengths in the along-track signal. We prefer here to smooth wavelengths beyond 500 km, which keep the baroclinic signal intact (the celerity of barotropic gravity waves, hence their wavelength, locally depends on square root of (gH), where H is the depth of the ocean. In the deep ocean, $H \approx 4000$ m, the typical wavelength of the barotropic M_2 tide is of the order of 9000 km, while the internal tide wavelengths are only of the order of 150–200 km). However, one must be aware that filtering might also remove some short-wavelength barotropic tidal structures, which certainly exist over ocean topographic features, as shown in hydrodynamic models, for example, the finite element solution (FES) models [*Le Provost et al.*, 1994].

[14] In order to remove the noise contained in the short-wavelength results, we also smoothed out very high frequencies. The instrumental noise is about 2–3 cm rms.

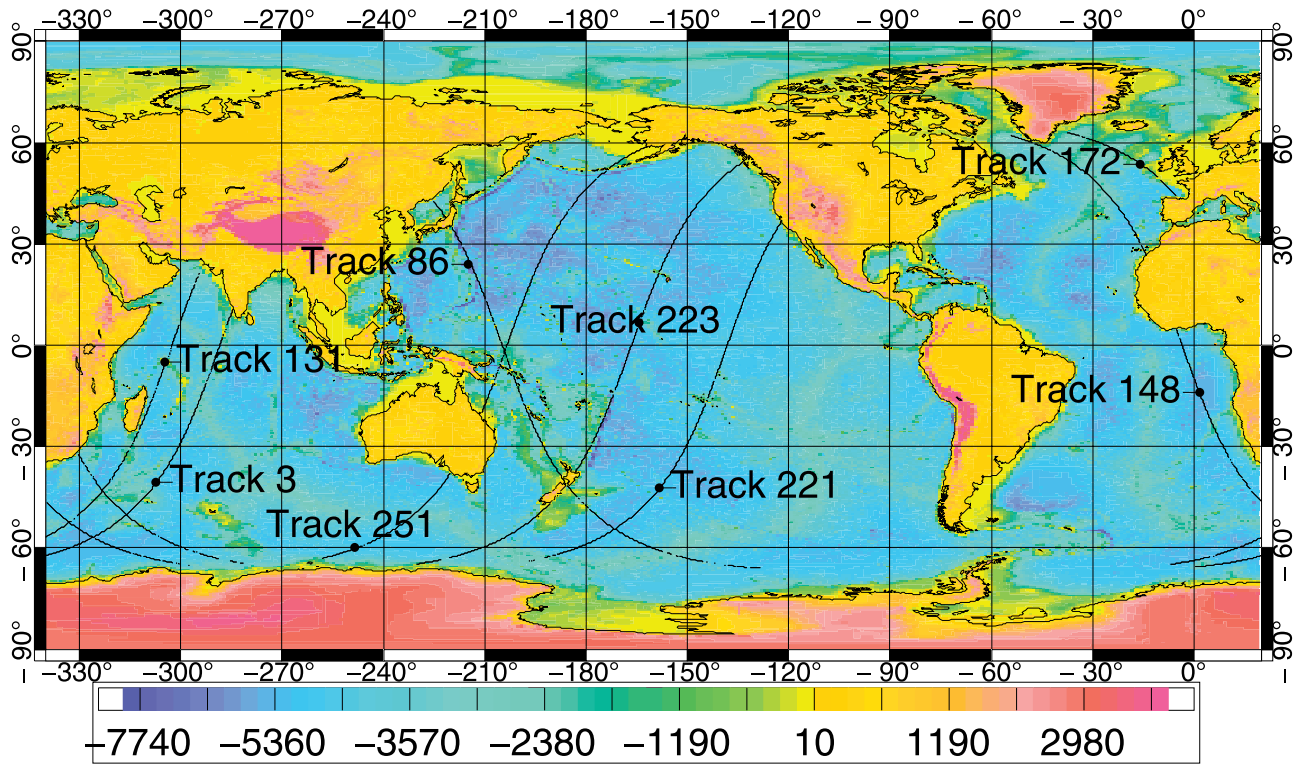

Figure 1. Location of the studied TOPEX/Poseidon (T/P) tracks, overlaying the ocean bottom bathymetry (scale in meters).

While filtering wavelengths lower than 50 km, this noise is reduced to less than 1 cm rms.

3. Analysis of Results for a Particular Typical Track

[15] Systematic analysis of T/P along-track data yields a huge amount of outputs. We first present hereafter the results for a particular track (track 221 CNES reference, see Figure 1) crossing the Pacific Ocean from the Southern Ocean to the Californian coast, through the Society Islands (Tahiti). We have performed the harmonic analysis of the T/P data every 7 km along this track for different periods and compared the results. Six periods have been analyzed for intercomparison: the first 7 years of T/P, the first 3 years, 3 and a half years, 4 years, 5 years, 6 years, and the last 3 and a half years of the 7 years considered.

[16] Figures 2 and 3show the along-track distribution of the M_2 characteristics, in amplitude A (Figure 2a) and in phase g (Figure 3a), as a function of latitude. On Figures 2 and 3, we show the results obtained from the analysis of the first 3 years (T1), the last 3 and a half years (T2), and the full 7 years (T0). We clearly see, superimposed over the large-scale signal of the barotropic tide, a short-wave signal identified by *Ray and Mitchum* [1997] to be the surface signature of internal tides. The most remarkable feature in this plot is the stability over time of the harmonic characteristics of the M_2 baroclinic signature in amplitude and phase. The major internal wave signal is centered on both sides of the Society Island chain (by 17°N).

3.1. Stability of Results for the Barotropic Tide

[17] We have low-pass filtered (Loess filter at a 500 km wavelength [*Schlax and Chelton*, 1992]) the along-track distribution of the M_2 amplitude and phase characteristics (real and imaginary parts), for the same three time spans T0, T1, and T2. As explained above, we consider that this filtered solution corresponds to the barotropic part of the full tidal signal. The results are shown on Figures 2b and 3b. If we recall the more recent tidal solutions [see *Le Provost*, 2001; *Ray*, 1999] and consider the amplitude of this wave along track 221, we know that from the Southern Ocean up to the U. S. west coast, we must go through two amphidromic points, by 20°S and 25°N, and cross an antiamphidromic bump at the equator. This is exactly what we observe on Figure 2b.

[18] The lower part of Figure 2b (scale on the right) shows the along-track amplitude of the "complex differences" between the M_2 barotropic tide obtained through harmonic analysis over the periods T1, T2, and T0: (T1−T0) is red; (T2−T0) is green. This "complex difference" includes both the differences in amplitude (A) and in phase (g) between the tidal characteristics obtained with the T0 and the T1 or T2 periods, respectively.

[19] These differences are at most of the order of 2 cm, the maximum values being located in areas of well-known strong ocean circulation variability: the Antarctic Circumpolar Current (ACC), between 60°S and 50°S, and the

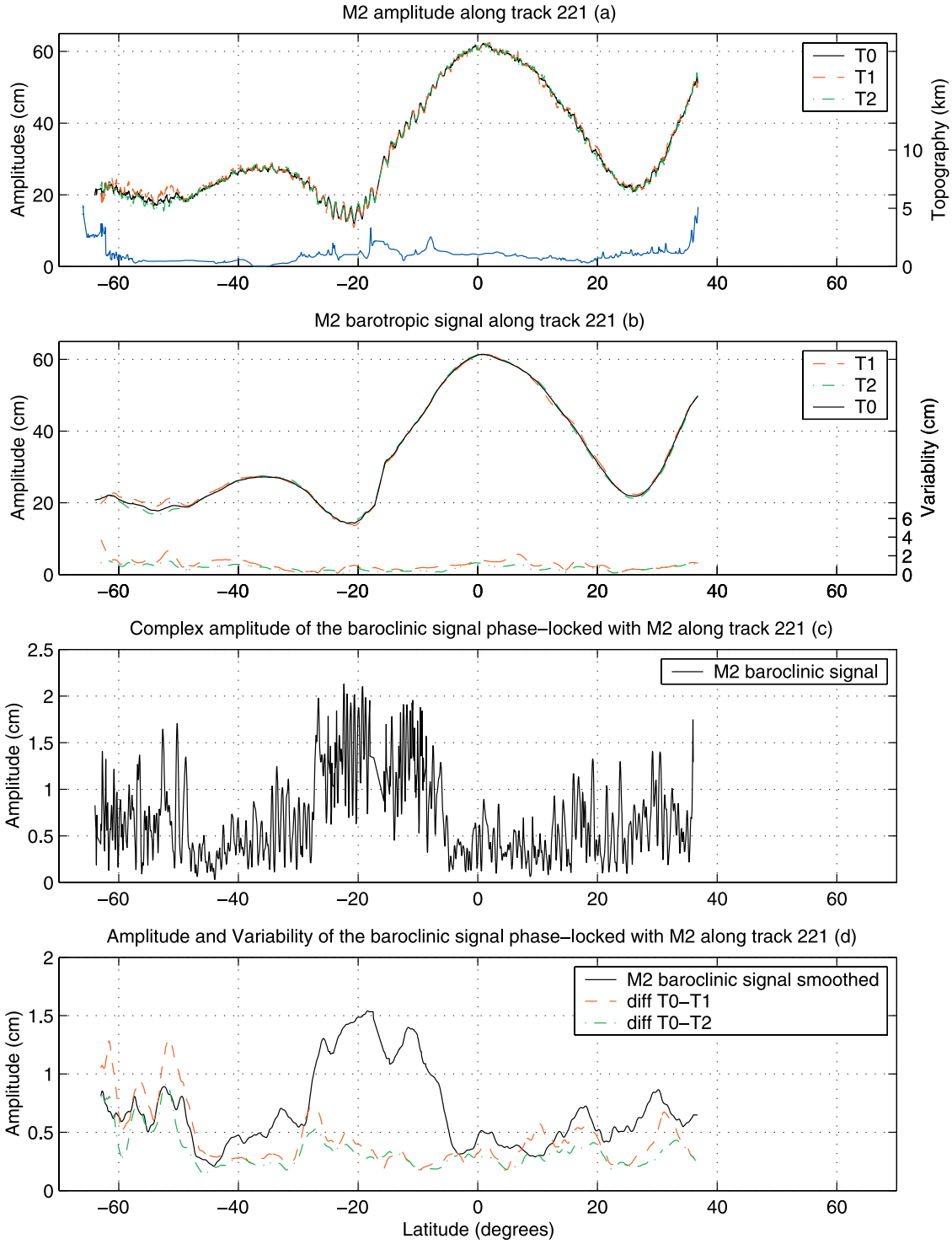

Figure 2. Amplitude of the barotropic and baroclinic signals along track 221 (over the Tahiti area). T0 is full T/P time series analyzed (1993–1999); T1 is first 3 years of T/P data (1993–1995); T2 is last 3 and a half years of T/P data (mid 1996–1999). (a) M_2 amplitude deduced from along-track harmonic analysis, bottom topography in blue. (b) Amplitude of the M_2 barotropic signal after low-pass filtering and variability of this barotropic signal (right scale). (c) Complex amplitude of the M_2 baroclinic signal. (d) Low-pass-filtered complex amplitude of the M_2 baroclinic signal and variability of this baroclinic signal.

Intertropical Convergence Zone (ITCZ), north of the equator. On Figures 2b and 3b, we can see that the differences are mainly in the amplitude of the wave in the ACC and the ITCZ areas. It is interesting to note that between the equator and 20°N, the maximum difference curve corresponds to the period T1, compared to T2; T1 does not include the major 1997 El Niño event in contrast to the periods T0 and T2. Notice that the El Niño impact on the sea surface dynamic

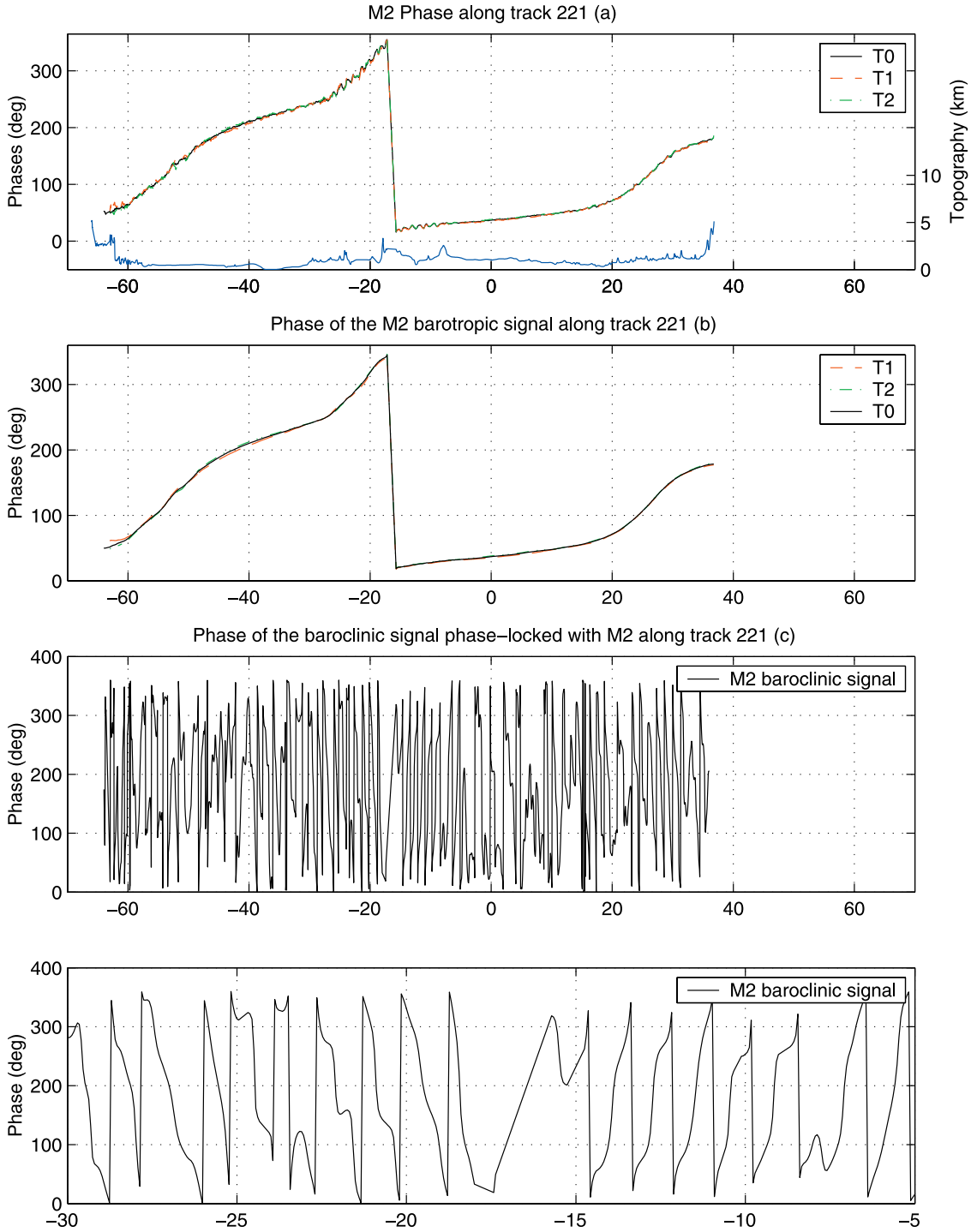

Figure 3. Phase of the barotropic and baroclinic signals along track 221 (over the Tahiti area). T0 is full T/P time series (1993–1999); T1 is first 3 years of T/P data (1993–1995); T2 is last 3 and a half years of T/P data (mid 1996–1999). (a) M_2 phase deduced from along-track harmonic analysis, bottom topography in blue. (b) Phase of the M_2 barotropic signal after low-pass filtering and variability of this barotropic signal (right scale). (c) Phase of the M_2 baroclinic signal with a zoom on the latitudes 30°S to 5°S.

topography is characterized by rather large spatial scales. We can conclude from this along-track analysis of the barotropic part of the M_2 tide that the results are stable over the T/P period at the centimeter level outside the zone of high ocean variability (here the ACC and the equatorial Pacific). As demonstrated by *Desai et al.* [1997] and others, the dominant source of error in the determination of the barotropic tide characteristics from satellite altimetry is the

ocean general circulation, which introduces higher noise levels in the areas of strong currents (Gulf Stream, Kuro Shivo, ACC, etc.).

3.2. Stability of the Signal for the Baroclinic Tides

[20] To investigate the characteristics of the M_2 baroclinic signal, we have subtracted the barotropic large-scale signal from the full signal. From Figure 2, we know that the amplitude of this signal is of the order of 5–6 cm "crest to trough" along this track in the vicinity of the Society Islands. This subtraction is done on the "real" and "imaginary" part of the along-track M_2 tidal characteristics (A cos g and A sin g). We show on Figures 2c and 3c the distribution along track of the amplitude and the phase, respectively, of this baroclinic signal. In such an along-track representation of the tidal wave characteristics, a purely traveling wave must be characterized by a constant amplitude (a plateau) and a phase distribution varying from 0° to 360° at the wavelength of the structure. In contrast, a purely standing wave must show a sinusoidal distribution in amplitude and a constant phase at half-wavelength scale.

[21] Along this track 221, we do not exactly see an amplitude plateau for the M_2 residual but rather a curve oscillating around an obvious plateau ranging from 0.5 to 1.5 cm (see Figure 2c). We can observe that the maximum amplitude values are located on both sides of the Society Island ridge, near 17°S. On the other hand, phases in this area exhibit an evident propagation on both sides, toward the north until ~5°S and toward the south until ~30°S (see Figure 3c). Thus the baroclinic signal isolated along this track is almost a traveling wave. The M_2 baroclinic signal appears spatially coherent in this area, with an evanescent distance of ~1100 km southward and ~1200 km northward. Notice that these decay scales, inferred from along-track plots, must be considered as a lower bound: accumulation of small variations in the propagation speed can cancel the internal waves signal over long distances, although this process is not considered as real dissipation [*Ray and Mitchum*, 1996]. The internal tides are dominated by the highest vertical modes [*Wunsch*, 1975]. Here, given the fact that the track 221 is perpendicular to the Society Island chain, it is reasonable to consider that the along track observed wavelength is the true one; we found that the semidiurnal baroclinic oscillations empirical wavelength is ~130 km. Notice that this value corresponds to the first baroclinic mode wavelength, about 120 km in the Tahiti area, deduced from a global first baroclinic mode map that we have calculated with the National Oceanographic Data Center (NODC) (Levitus) World Ocean Atlas 1998 data set (National Oceanic and Atmospheric Administration-Cooperative Institute for Research in Environmental Sciences (NOAA-CIRES) Climate Diagnostics Center, Boulder, Colorado, U. S. A., available at http://www.cdc.noaa.gov/, hereinafter referred to as NODC (Levitus) World Ocean Atlas 1998) and the Sturm-Liouville equation. The Sturm-Liouville eigenvalues problem involves the stratification of the ocean through the buoyancy frequency term, which when squared gives a clue about the stability of the environment: If positive, the medium is stable; if negative, it is unstable [*Gill*, 1982]. The stratification of the ocean is very important for the generation and propagation of internal waves. The northern limit (~5°S) of the propagation of the internal waves coming from the Tahiti region is likely explained by a steep bump in the bottom topography at 8°S, and the temporal variability of the oceanic stratification; in the equatorial Pacific, the stratification of the ocean becomes close to a two-layer ocean and is strongly affected by the El Niño–La Niña events. At high latitudes (beyond 35°S and 35°N), the ocean stratification also changes and becomes more stirring [*Guilyardi*, 1997; NODC (Levitus) World Ocean Atlas 1998]. A temporal modification of the stratification added to other dissipative processes (temporal variability of the oceanic medium, rough bathymetry, reflection and interferences between different internal wave trains, internal turbulent friction, wave breaking [cf. *Wunsch*, 1975]) implies the vanishing of these baroclinic tides.

[22] To further investigate the temporal statistical stability of the baroclinic internal tide signal along track 221, we have carried out similar decompositions on the results of the harmonic analysis made over the different time spans (T0, T1, T2, etc.). The end results are very similar and stable over the area of well-identified presence of internal tide between 5°S and 30°S in terms of amplitude, phase, and characteristic wavelengths.

[23] To characterize this "stability," we have smoothed (at 500-km wavelength) the along-track distribution of the M_2 baroclinic amplitude characteristics for the same three time spans T0, T1, and T2. The result in amplitude A_f(T0) is shown on Figure 2d for the T0 period; this filtered curve gives the order of magnitude of the traveling part of the baroclinic wave along track. The phase g_f (T0) is plotted on Figure 3c, with a zoom on the 30°S–5°S latitudes on the last panel of Figure 3; we clearly see the wave propagation away from the island in this region. On Figure 2d, we also display the "complex difference" of the filtered baroclinic M_2 wave characteristics derived from the analysis of the T0 period and the T1 and T2 periods, respectively. Figure 2d illustrates the stability of the baroclinic signal in the area 30°S–5°S. We quantify this stability through the ratio

$$\mathrm{S/N} = A_f(\mathrm{T0})/A_f(Tx - \mathrm{T0}).$$

The S/N ratio found in this area reaches 4.6. The largest values are concentrated around the islands, near 17°S, and they decrease moving away, in corroboration with the decay distances. This S/N ratio is thus a good index of the level of temporal statistical stability of the baroclinic signal. These findings are astonishing because internal waves characteristics are strongly dependent on the ocean stratification, which varies over time. The stability of this baroclinic signal over time is likely related to the stability of the first internal mode of the ocean [*Chelton et al.*, 1998].

4. Generalization to the Global Ocean

[24] These along-track analyses on the global ocean have been completed for the different time periods mentioned above. Then the results have been high- and low-pass filtered, as described in section 2. All these results have been collected in bins of 1° × 1°, which allows us to

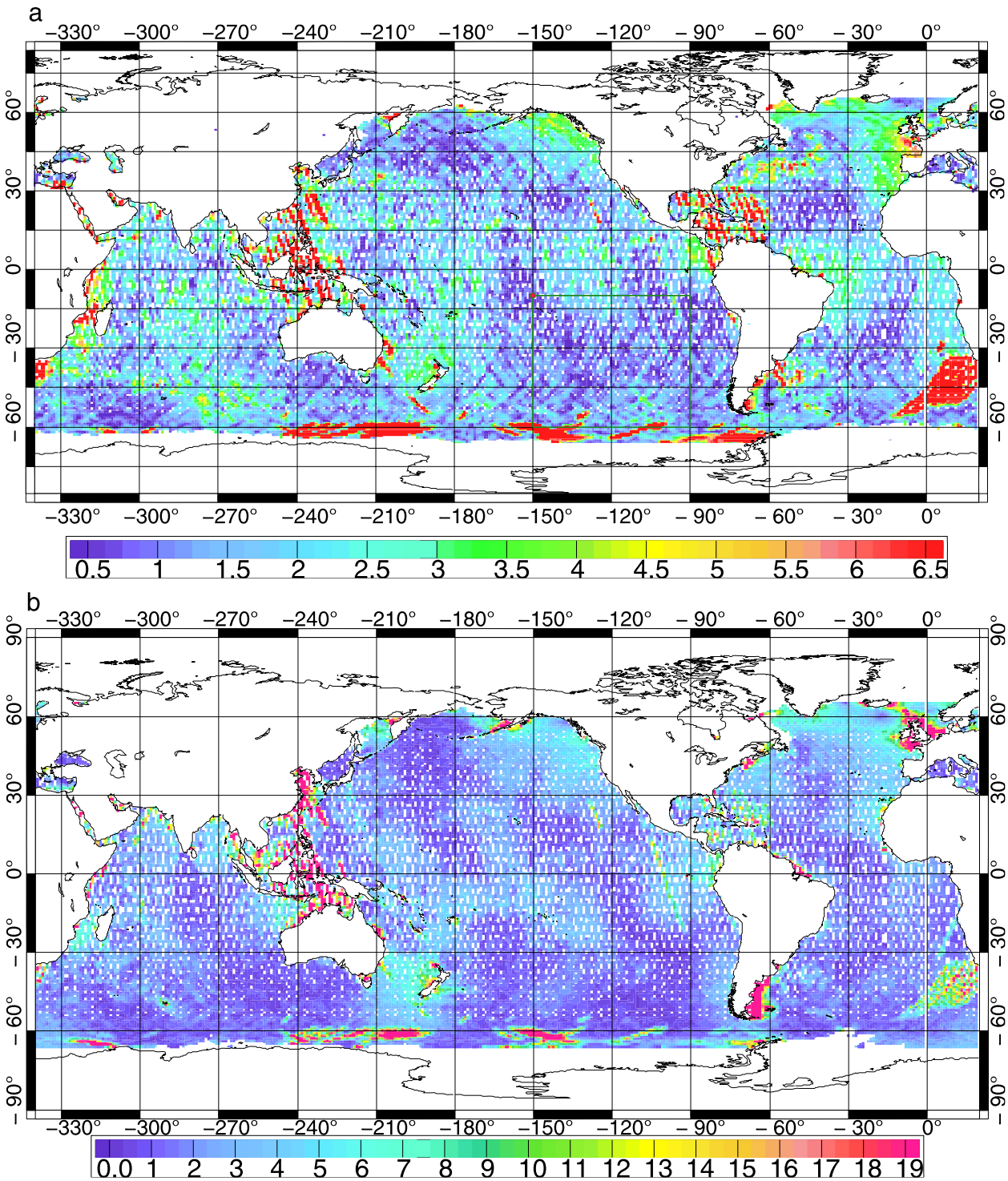

Figure 4. Global charts of the M_2 barotropic signal deduced from T/P altimetry. (a) Variability of this M_2 barotropic signal in centimeters. (b) Amplitude of the complex difference between the M_2 altimetric map and the FES 2002 M_2 wave.

visualize the results on color maps as presented in Figures 4 and 5, composed of $1° \times 1°$ pixels.

4.1. Barotropic Signal and Its Temporal Stability

[25] First, to gain an overview of the results at a global scale, we have derived global maps of the semidiurnal M_2 tide (amplitude and phase), after along-track 500-km filtering, for each of the periods analyzed (T0, T1, T2). These maps (not shown) are very similar to the standard solutions produced recently [*Le Provost*, 2001; *Ray*, 1999], at least qualitatively.

[26] The "complex difference" between these solutions (from periods T1 and T2) has been computed. We present on Figure 4a the mean over each $1° \times 1°$ pixel of these

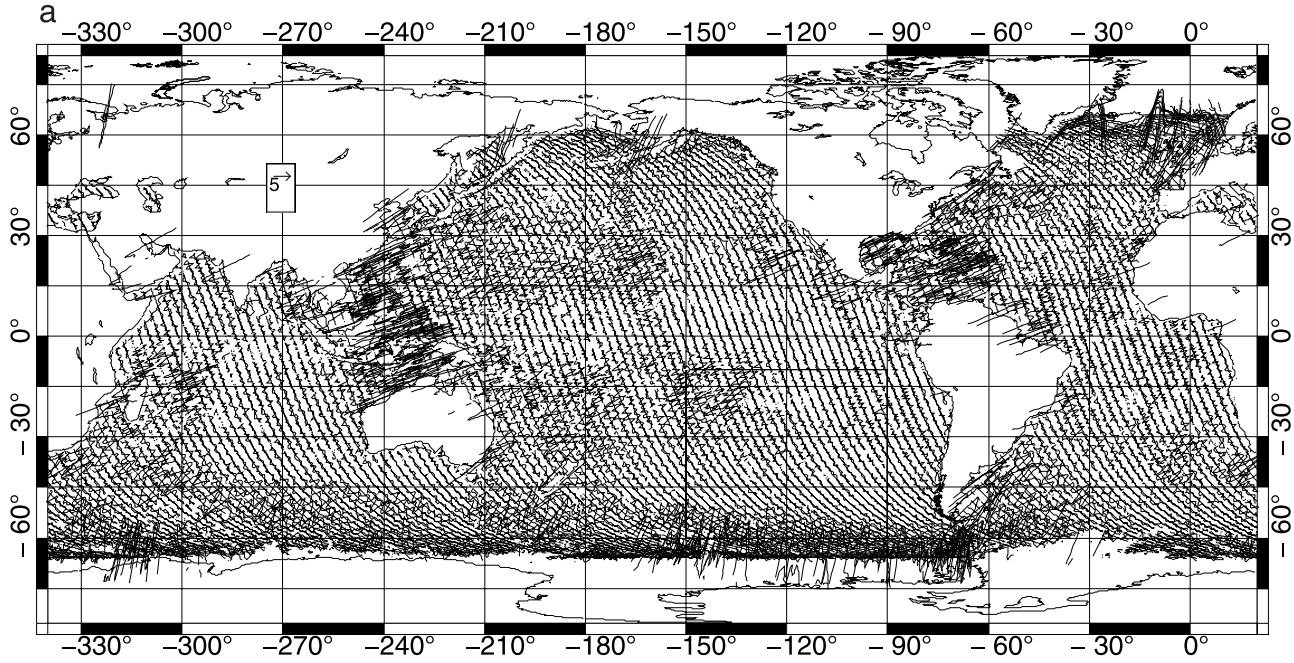

Figure 5. Global charts of the M_2 baroclinic signal deduced from T/P altimetry. (a) M_2 baroclinic amplitude along T/P descending tracks in centimeters. (b) Variability of this M_2 baroclinic signal in centimeters. (c) Signal-to-noise ratio for the M_2 baroclinic tide deduced from T/P altimetry.

complex differences. They are the two-dimensional equivalent of the lower curves displayed on Figure 2b. Differences are lower than 1 to 2 cm in most regions.

[27] 1. Over the large oceanic current areas like the Gulf Stream, the Brazil Malvinas convergence, and the ACC, the differences range from 3 to 6 cm; this is the consequence of the high level of noise introduced in the altimeter signal by aliasing of the mesoscale variability, as pointed out by *Desai et al.* [1997], *Tierney et al.* [1998], and others.

[28] 2. Differences of the order of 3 to 4 cm are also noticeable over the areas where the M_2 tide is large over the three ocean basins: the Atlantic Ocean (the far north and northeast Atlantic, the western part of the equatorial Atlantic), the Pacific Ocean (the far northeastern part close to the coast of Alaska, around New Zealand, and over the antiamphidromes of the west, central, and east equatorial Pacific), and the Indian Ocean (over the central antiamphidrome of this basin, and west of Madagascar, in the Mozambique Channel). It is, however, important to note that over all these areas, the "complex difference-to-M_2 amplitude" ratio is below 0.03.

[29] 3. Finally, we should note that over the continental shelves these differences are of the order of 5 to 6 cm.

[30] Red spots in the Southern Ocean may correspond to ice-covered areas, which induce more scattered (in time and in space) altimeter time series. What is happening southeast of Africa is probably due to some errors during the processing of the T/P time series. The greater variability observed in the Gulf of Mexico and in the Indonesian Seas can be explained by the large number of small islands in these areas that make T/P measurements more uncertain and thus time series more scattered. Moreover, the baroclinic variability is apparently nonnegligible in this last region, which might bias the T/P data analysis; the Gulf of Mexico and the Indonesian Seas are characterized by a quite low signal-to-noise ratio, although their topographic configuration is favorable to internal wave generation (see section 4.3). Outside these limited areas, the effective stability of the barotropic signal is thus verified.

[31] Although these along-track estimates show a clear temporal stability, they remain a bit more noisy than expected for the barotropic tide; our findings corroborate previous ones [*Tierney et al.*, 1998] that many different oceanographic signals may corrupt these barotropic estimations, ranging from nontidal signals with a period close to 60 days, the aliasing period of M_2, to T/P instrumental noise, mesoscale variability, the existence of noncoherent baroclinic tides, and the possible temporal variability of the M_2 harmonic tidal constituent itself. Note that all these sources of variability in the determination of the harmonic tidal constants have been partially canceled out in the more usual approach (not along-track analysis) applied to derive tidal solutions from and for satellite altimetry [*Le Provost*, 2001]. This has been done by combining neighboring data from neighboring tracks, by using the extra information available at crossovers, or by using dynamics models. The major advantage of these along-track estimates, although more noisy, is that they retain the short-wavelengths tidal features, which do not appear in the usual global models. Furthermore, along-track estimates must give results nearly as accurate in shallow waters as in the deep ocean, which is not true for the usual hydrodynamic and empirical models [*Andersen*, 1999; *Tierney et al.*, 2000].

4.2. Similarities With the Standard Finite Elements (FES) and Global Ocean Tide (GOT) Solutions

[32] An interesting comparison is to compute the complex differences between these purely altimetric barotropic

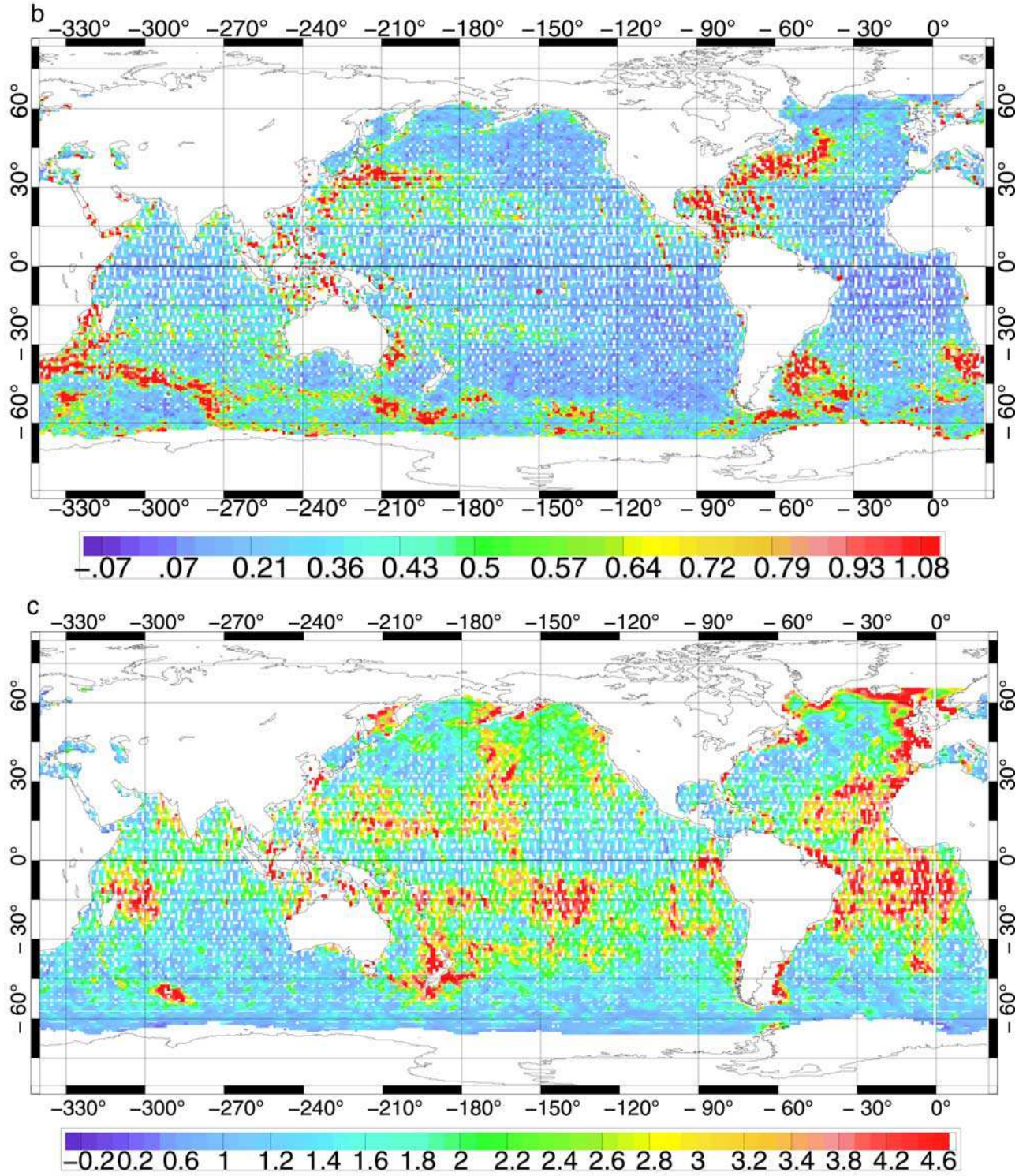

Figure 5. (continued)

maps and maps derived from the FES 2002 (high-resolution version of FES 99 [*Lefèvre et al.*, 2002]) and GOT 99.2 [*Ray*, 1999] tidal models. On Figure 4b, we present the amplitude of the vector difference between one of these solutions and FES 2002. Over the deep ocean, the difference remains below 5 cm, indeed closer to 1 cm on the global ocean. There are of course some areas where the difference can reach 10–20 cm: between Indonesia and Australia, in the Yellow Sea, in the English Channel and the North Sea, South of Brazil and beyond latitudes 60°N and 60°S. The problem of determining the boundary between ice and water in the Antarctic is also apparent in the red spots south of 60°S. The differences located southeast of Argentina, at the mouth of the Amazon, on

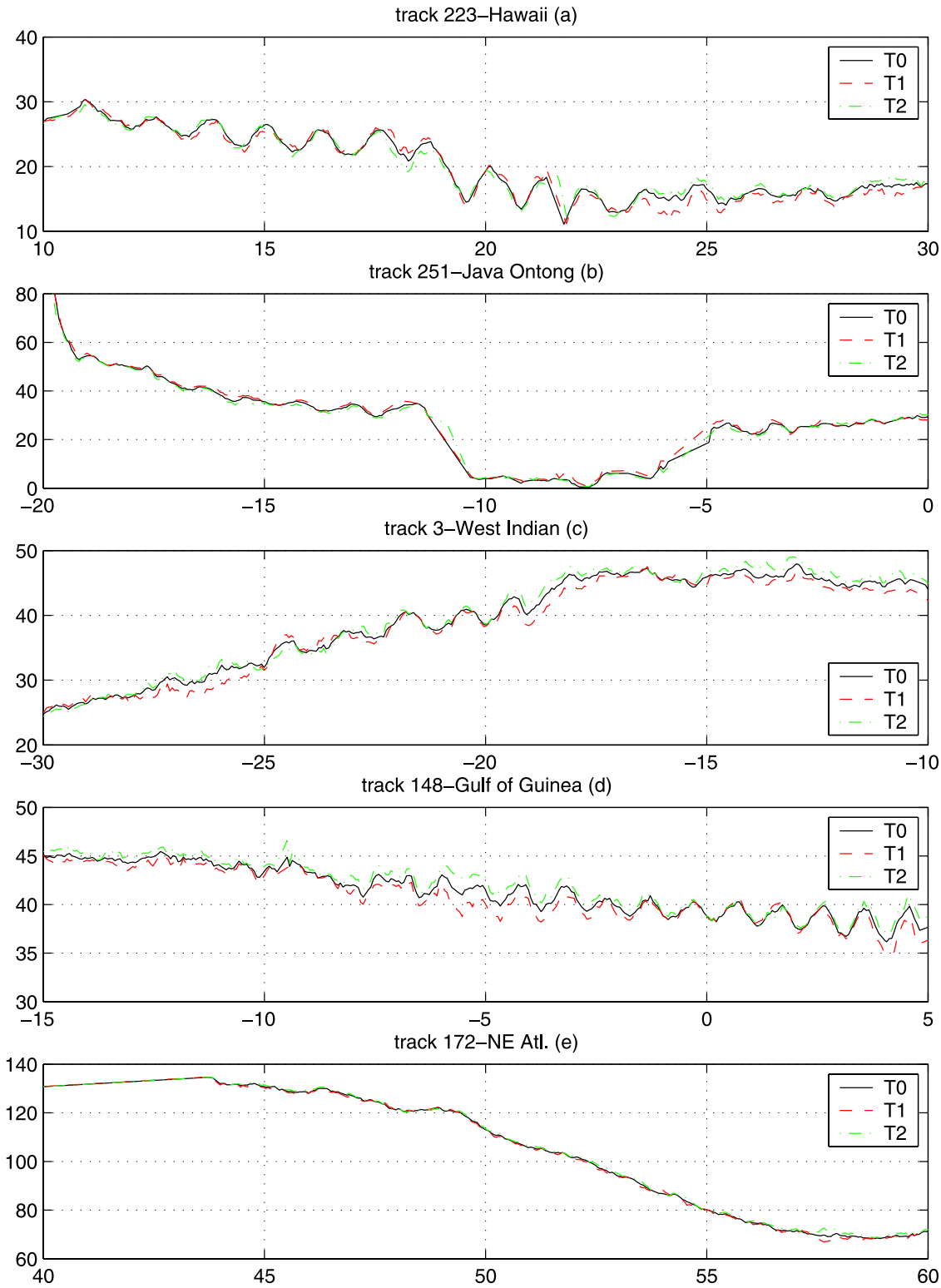

Figure 6. Zoom on five areas where internal wave signatures appear in T/P measurements. Amplitude of the along-track M_2 signal (barotropic plus baroclinic) is in centimeters. (a) Track 223 over the Hawaii chain. (b) Track 251 over the Java-Ontong plateau. (c) Track 3 over the west Indian Ocean. (d) Track 148 over the Gulf of Guinea. (e) Track 172 in the northeast Atlantic.

the European Continental shelf, in the Yellow Sea, and in the Indonesian Seas, are certainly, in part, symptomatic of the fact that models are less efficient in shallow waters. The differences in the Indonesian Seas are also probably emphasized by the greater variability observed in T/P data analysis in this area.

4.3. Baroclinic Signal and Its Stability

[33] To investigate the baroclinic signal and its temporal stability, we have computed for the different time spans T0, T*x*,. . . two sets of global maps, one for the ascending tracks and the other for the descending tracks, representing the along-track difference between the point-to-point M_2 amplitudes and the 500-km smoothing. One such map (descending tracks) is shown on Figure 5a. These maps allow us to locate the areas where either the noise-to-signal ratio is high (the large ocean currents) or the areas where internal tides are significant. The major areas of intense baroclinic signal are easy to see: (1) the Mascaren ridge east of Madagascar, the Maldivian ridge, the Ninety East ridge and Carlesberg ridge in the northern Indian Ocean, (2) the Kusu-Palau ridge south of Japan, the Hawaiian island chain, the Tuamotu and the Society archipelagos, the Mendocino ridge off the west coast of the United States, (3) the Melanesian and the Micronesian island chains in the western equatorial Pacific, the Macquarien ridge south of New Zealand, (4) the Reykjanes ridge south of Iceland, the Great Meteor Banks in the North Atlantic, (5) the ridge off Trinidad east of Brazil, and the Walvis ridge in the South Atlantic Ocean.

[34] These maps display features very similar to those presented by *Kantha and Tierney* [1997] and only computed with about 3 years of T/P data at that time. The results in the Hawaii region also show striking similarities with those obtained by *Ray and Mitchum* [1997], although once again the analyses are computed on very different time spans. This confirms that the baroclinic signal is very stable there.

[35] Let us now focus on the results of the first 3 years (T1) of data and then the last 3 and a half years (T2), and compare them to the T0 time span. As explained above, this choice enables us to investigate distinct time periods covering in particular different climate conditions (El Niño period). The global map representing the amplitude of the ''complex difference'' between these computations is given on Figure 5b, interpolated on a $1^\circ \times 1^\circ$ grid. The areas of high temporal variability are clearly visible (amplitude higher than 1.1 cm, in red on the maps) due to the large oceanic currents, such as the Gulf Stream, the Kuroshio Current, the Brazil Current, the West Australian Current, the CCA, and so on. In contrast, it is not possible to identify on Figure 5b the regions where we previously noticed the presence of potentially true baroclinic signals; they are located in the blue-green areas corresponding to an amplitude difference lower than 0.5 to 0.1 cm, for example, the areas around Hawaii and Papeete.

[36] To identify the areas where the coherent baroclinic signal is stable over time, we have thus computed everywhere along the tracks the signal-to-noise ratio previously mentioned. The result is displayed on Figure 5c. The main regions of intense baroclinic signatures are clearly shown on this map, and they are located around Tahiti, Hawaii, the Guinea Gulf, the northeast Atlantic, the Mascaren ridge, the mouth of the Amazon, and off the coast of Chile.

[37] This map contains important new information, since it identifies the areas over the global ocean where the coherent part of the baroclinic M_2 tidal wave propagates from source points, where the barotropic tidal currents interact with particular topographic features.

[38] Our aim here is not to further investigate all these areas. We will focus on a few locations in order to illustrate their different characteristics.

4.3.1. Areas Already Well Studied From in Situ Data and Altimetry

4.3.1.1. Hawaii

[39] The baroclinic signal around Hawaii (23°N) is easy to notice on Figure 5; its amplitude reaches 6.8 cm ''crest to trough'' (see Figure 6a). The tide-coherent baroclinic signal has been extensively analyzed by *Ray and Mitchum* [1997], who demonstrated that these oscillations are effectively the surface signature of the internal waves generated by the barotropic tide current flowing over the Hawaiian ridge. Let us point out the major characteristics that we similarly observe in our results and which appear to be temporally very stable. We focus on ascending track 223 (Figure 6a). The complex amplitude oscillates around 2 cm and grows to ~4 cm toward Hawaii Island. There is an evident phase propagation, particularly south of the island, where one can estimate the wavelength to about 141 km. North of the island along track 223, the propagative signal is weaker (wavelength of 135 km), but it confirms previous in-situ studies results [*Ray and Mitchum*, 1997; *Dushaw et al.*, 1995; *Chiswell*, 1994], which showed very clear internal tide records in this area. The M_2 barotropic currents are coming from the north-northeast in this region [*Le Provost et al.*, 1994], and the topography north of the ridge along track 223 is complex. The evanescent distance of these waves reaches nearly 2000 km southward and northward as already inferred by *Dushaw et al.* [1995]. Figure 5b reveals that these internal tide signatures are quite steady around the Hawaii chain. This area corresponds to a signal-to-noise ratio greater than 3.

4.3.1.2. Java-Ontong Plateau

[40] *Gourdeau* [1998] studied a region on the Java-Ontong plateau (at 2°S–156°E) where internal tides are easily spotted. Thanks to two pressure gauges at depths of 300 and 500 m, and an Autonomous Temperature Line Acquisition System (ATLAS) placed between 25 and 500 m, the COARE experiment, from September 1992 to February 1993, spotted semidiurnal internal waves propagating northeastward and with a high temporal variability. These waves are likely generated on the large sloping topography between the Kilinailau Trench and the Java-Ontong plateau. These experimental results were also validated by the analysis of a few cycles of T/P data (cycles 2 to 15, which cover the same temporal period) in this area, restricted to 0°S to 6°S. The characteristic wavelengths were then estimated to 100–150 km for a calculation along ascending track 251 and to 250 km for descending track 86. Our approach also reveals interesting baroclinic oscillations in this region, around 2.5°S–156°E, with a ''crest to trough'' amplitude of 4.7 cm for ascending track 251 (see Figure 6b). For descending track 86, which has a more tangential angle of incidence with respect to the relief, the signal is less obvious and the amplitude only reaches 2 cm. A power spectrum analysis of the M_2 baroclinic elevation along these two tracks, taking into account cycles 11 to 255,

gave wavelength characteristics similar to those suggested by *Gourdeau* [1998]: 200-km wavelength for track 86 and about 120 km for track 251. Our results, although computed over a longer time period of about 7 years, are very close to those of Gourdeau computed only over a 5-month period. The signal seems to be fairly stable. However, the rather low signal-to-noise ratio, about 2, suggests that we should be careful here, because although the altimeter detects internal waves signatures, the signal is often underestimated.

4.3.2. Areas of Complex Topography, Not Normal to T/P Tracks

4.3.2.1. Walvis Ridge

[41] Southwest of Africa, the baroclinic coherent signal reveals the existence of internal waves; the amplitude is 1.5 cm at about 40°S, where we know there is a submarine ridge expanding from southwest to northeast. However, probably owing to the fact that T/P tracks do not cross this relief at right angles, the signal remains rather weak in this area.

4.3.2.2. Gulf of Guinea

[42] In the Gulf of Guinea, the internal tide signature is clearly revealed by our altimetric approach. In this region, the exciting relief is the African coastline of the Ivory Coast. The signal is difficult to spot on the global maps: Satellite tracks do not cross the shelf break at right angles so the altimeter measurements probably underestimate the internal wave signal. The signal is stronger on the descending tracks. A close-up of track 148 (Figure 6d) shows the characteristics of the baroclinic signal in this area: short-wavelength oscillations of about 95 km and 5–6 cm "crest to trough," which propagate until approximately 1400 km southward. This wavelength is coherent with the theoretical first baroclinic mode in the area, which is ~90 km. The stability of the baroclinic signal detected here is really striking. The high values of the signal-to-noise ratio, reaching more than 4.6, also support the presence of a stable M_2 coherent baroclinic signal in this region. Note, however, the long-wavelength differences between T0, T1, and T2 analysis, which correspond to the variability of the T/P barotropic M_2 signal, as shown in Figure 4a.

4.3.2.3. West Indian Ocean

[43] In addition to the Mascaren ridge region where internal tides have already been studied [*Morozov*, 1995], some interesting internal wave signatures are noticeable northeast of Madagascar (latitudes 8°S to 20°S and longitudes around 50°E); the baroclinic signal has a crest to trough amplitude of 3.5 cm along track 131 and a wavelength of 157 km. The Seychelles' chain constitutes the major topographic feature of this area, which favors internal waves generation, particularly since this region is also characterized by a minimum of M_2 amplitude and thus by high barotropic currents.

[44] Track 3 (Figure 6c), nearly perpendicular to the mid-Indian ridge, also shows very strong and stable oscillations with an amplitude of 2–3 cm, between latitudes 18°S and 25°S. The wavelength of these internal tides is 131 km. The signal-to-noise ratio is strong in this region of the western Indian Ocean, about 4, which corroborates the stability of these baroclinic waves.

4.3.3. Areas of More Complex Internal Tide Systems

4.3.3.1. Northeast Atlantic

[45] A region well known to be susceptible to generating internal waves is the European shelf break in the northeast Atlantic. We would thus expect to detect a quite large and coherent signal there. Yet this is not the case. In this area, our along-track analysis does not reveal any very clear oscillation (track 172 on Figure 6e). This signal's low temporal coherence is likely to explain the poor information given by T/P data in this region. This lack of temporal coherence is supported by the study of *New* [1988] in the Bay of Biscay, which showed that baroclinic mode 3 dominates the displacements seaward of the shelf slope. These higher-order modes are very sensitive to stratification changes and thus they have a greater temporal variability. Consequently, the fact that their characteristics are not stable prevents them from being well detected by the altimetry. Moreover, the wavelengths are of the order of 50 km off the Bay of Biscay [*Pingree and New*, 1995]. We have filtered very high wavelength signals (cut off at 50 km) from our analysis, so the third-mode baroclinic signal that likely exists in this area has also probably been removed. However, an interesting feature on Figure 5b is the high signal-to-noise values on the European continental shelf, which suggests that a fairly strong and stable signal exists. At this stage, analysis of the noncoherent baroclinic signal would be worth expanding in this region of the European shelf break. However, this is not within the scope of this study.

4.3.3.2. Other Areas

[46] One also notices other interesting areas with fairly clear oscillations north of Brazil off the Amazon shelf, and weaker oscillations near the Cape Verde Islands, in the Atlantic Ocean, or off the Chilean coast in the Pacific. These patterns are less spatially coherent compared to the large propagating patterns found around Hawaii, Tahiti (see section 3.2 on track 221), or the Gulf of Guinea. A very complex ridge pattern in the region north of Brazil may explain this low spatial coherence. Off Chile, a strong barotropic tide arrives southward on the Nazca ridge, but satellite tracks are not at the right angle to the topography to let us see all the generated oscillations in all directions. Nevertheless, the signal-to-noise ratios of around 4 suggest that the internal tides in these regions are very stable.

5. Conclusion

[47] As noted in section 1, the aims of this paper were (1) to investigate the convergence (as a function of the length of the analyzed time series) and stability (over time) of the tidal characteristics deduced from along-track analysis of the T/P data and (2) to locate the areas where these characteristics are the most stable.

[48] We considered the first 7 years of T/P. The methodology was to divide this T/P data set into periods of 3 years or more (at least 3 years are required to overcome the aliasing problem due to the 10-day T/P cycle). Over each period, the along-track characteristics of the M_2 tide have been computed through harmonic analysis. We have focused on the variability of these M_2 tidal characteristics as a function of the window of analysis. Surprisingly, the results appear to be very stable over the studied period, over many areas of the global ocean.

[49] For the barotropic component, as expected, these along-track estimates are temporarily stable, with, however, a certain degree of variability ranging from less than 1 cm

up to 6 cm. This is much larger than physically acceptable. The spatial distribution of this variability identifies its main origins, which are the noise induced by the mesoscale ocean circulation, and the difficulties in overcoming the aliasing problem, directly proportional to the amplitude of the other tidal components (mainly S2).

[50] Comparison between this along-track solution and the more recent solutions proposed in the literature (GOT99.2 and FES2002) reveals that the differences are very low, a few centimeters at most, except over the continental shelves. There the differences exceed by far the dispersion related to the different time spans used for the along-track analysis. It is recognized that there is still room for improvement of these global solutions like GOT99 and FES2002 over the continental shelves. The level of stability of the tidal characteristics deduced from along-track analysis holds out the possibility of improving accuracy in coastal areas by using altimetric data.

[51] More surprising is the stability of the results obtained for the characteristics of the M_2 baroclinic signal. With only 3 years of data, *Ray and Mitchum* [1997], *Kantha and Tierney* [1997], and others discovered that along-track analysis of T/P data allows us to detect the surface signature of the part of the internal tides that maintains coherency with the astronomical forcing. The results presented here reveal that the characteristics of this signal, in amplitude and phase, are very stable over the period 1993–1999, over the areas of major baroclinic signal. As we noticed, this stability along with time is likely related to the stability of the first internal mode of the ocean. We have introduced an index (S/N ratio) to characterize the level of temporal stability of the M_2 baroclinic signal. This allows us to map the regions where the baroclinic signal is significant and stable over time. This map is an innovative piece of information. It pinpoints the areas of the global ocean where the coherent part of the baroclinic M_2 tidal waves propagates from the source locations where the barotropic tidal currents interact with topographic features. This map is potentially of interest for ocean modelers, indicating the regions where the scattering of the barotropic tides into mode one waves is efficient and tidal mixing may be weak. It could also be of interest for assimilating altimetric data: In these regions of significant and stable tidal baroclinic signal, the error bars on the along-track data must take into account the space and time aliasing of this signal. We must, however, keep in mind that these results are dependent upon the orientation of the satellite track with respect to the direction of propagation of the internal waves, and also on the along-track and intertrack resolution with respect to the wavelength characteristics of the internal wave signal. The new T/P data obtained in recent months along a new track midway between adjacent Jason-1 ground tracks could provide particularly valuable information on this problem, provided that periods of observation by the two satellites are long enough for us to deconvolute the different components of the tidal signal in the semidiurnal band and allow a clear extraction of the M_2 signal.

[52] This study was limited to the M_2 tide. It could be that similar results would be obtained for the other major tidal components. However, the signal-to-noise ratio is such that longer time series are required to investigate the stability of S_2 or N_2. Such studies are required to investigate the feasibility of an internal tide correction to be included in future satellite data processing systems. Besides, the noncoherent baroclinic signal from the satellite altimetry database is yet to be studied.

References

Andersen, O. B. (1999), Shallow water tides in the northwest European shelf region from TOPEX/Poseidon altimetry, *J. Geophys. Res.*, *104*(C4), 7729–7741.

Chelton, D. B., R. A. Deszoeke, M. G. Schlax, K. El Naggar, and N. Siwertz (1998), Geographical variability of the first baroclinic Rossby radius of deformation, *J. Phys. Oceanogr.*, *28*, 433–460.

Chiswell, S. M. (1994), Vertical structure of the baroclinic tides in the central North Pacific subtropical gyre, *J. Phys. Oceanogr.*, *24*, 2032–2039.

Desai, S. D., J. M. Wahr, and Y. Chao (1997), Error analysis of empirical ocean tide models estimated from Topex/Poseidon altimetry, *J. Geophys. Res.*, *102*(C11), 25,157–25,172.

Dushaw, B. D., B. D. Cornuelle, P. F. Worcestor, B. M. Howe, and D. S. Luther (1995), Barotropic and baroclinic tides in the central North Pacific Ocean determined from long-range reciprocal acoustic transmissions, *J. Phys. Oceanogr.*, *25*, 631–647.

Gill, A. E. (1982), *Atmosphere-Ocean Dynamics*, 662 pp., Academic, San Diego, Calif.

Gourdeau, L. (1998), Internal tides observed at 2°S–156°E by in-situ and TOPEX/Poseidon data during the Coupled Ocean-Atmosphere Response Experiment (COARE), *J. Geophys. Res.*, *103*(C6), 12,629–12,638.

Guilyardi, E. (1997), Rôle de la Physique Océanique sur la Formation/Consommation des Masses d'Eau dans un Modèle Couplé Océan-Atmosphère, Ph.D. thesis, Univ. Paul Sabatier, Toulouse, France.

Kantha, L. H., and C. C. Tierney (1997), Global baroclinic tides, *Prog. Oceanogr.*, *40*, 163–178.

Lefèvre, F., F. H. Lyard, C. Le Provost, and E. J. O. Schrama (2002), FES99: A global tide finite-element solution assimilating tide gauge and altimetric information, *J. Atmos. Oceanic Technol.*, *19*, 1345–1356.

Le Provost, C. (2001), Ocean tides, in *Satellite Altimetry and Earth Sciences*, edited by L. L. Fu and A. Cazenave, pp. 267–303, Academic, San Diego, Calif.

Le Provost, C., M. L. Genco, F. Lyard, P. Vincent, and P. Canceil (1994), Spectroscopy of the world ocean tides from a finite-element hydrodynamic model, *J. Geophys. Res.*, *99*(C12), 24,777–24,798.

Le Provost, C., A. F. Bennett, and D. E. Cartwright (1995), Ocean tides for and from TOPEX/Poseidon, *Science*, *267*, 639–642.

Morozov, E. G. (1995), Semi-diurnal internal wave global field, *Deep Sea Res., Part I*, *42*, 135–148.

New, A. L. (1988), Internal tidal mixing in the Bay of Biscay, *Deep Sea Res., Part A*, *35*, 691–709.

Pingree, R. D., and A. L. New (1995), Structure seasonal development and sunglint spatial coherence of the internal tide on the Celtic and Armorican shelves and in the Bay of Biscay, *Deep Sea Res., Part I*, *42*, 245–284.

Ponchaut, F., F. Lyard, and C. Le Provost (2001), An analysis of the tidal signal in the WOCE Sea Level Dataset, *J. Atmos. Oceanic Technol.*, *18*, 77–91.

Ray, R. D. (1999), A global ocean tide model from TOPEX/Poseidon altimetry: GOT99.2, *NASA Tech. Memo.*, *209478*, 58 pp.

Ray, R. D., and G. T. Mitchum (1996), Surface manifestation of internal tides generated near Hawaii, *Geophys. Res. Lett.*, *23*(16), 2101–2104.

Ray, R. D., and G. T. Mitchum (1997), Surface manifestation of internal tides in the deep ocean: Observations from altimetry and island gauges, *Prog. Oceanogr.*, *40*, 135–162.

Schlax, M. G., and D. B. Chelton (1992), Frequency domain diagnostics for linear smoothers, *JASA J. Am. Stat. Assoc.*, *87*(420), 1070–1081.

Schrama, E. J. O., and R. D. Ray (1994), A preliminary tidal analysis of TOPEX/Poseidon altimetry, *J. Geophys. Res.*, *99*(C12), 24,799–24,808.

Tierney, C., M. E. Parke, and G. H. Born (1998), An investigation of ocean tides derived from along-track altimetry, *J. Geophys. Res.*, *103*(C5), 10,273–10,287.

Tierney, C., L. H. Kantha, and G. H. Born (2000), Shallow and deep-water global ocean tides from altimetry and numerical modeling, *J. Geophys. Res.*, *105*(C5), 11,259–11,277.

Wunsch, C. (1975), Internal tides in the ocean, *Rev. Geophys.*, *13*, 167–182.

L. Carrère, C. Le Provost, and F. Lyard, Laboratoire d'Etude en Géophysique et Océanographie Spatiales, Unite Mixte CNRS-CNES-IRD-UPS, Observatoire Midi Pyrénées, 18 Av. E. Belin, 31401 Toulouse Cedex 4, France. (carrere@notos.cst.cnes.fr)